ACS APPLIED MATERIALS & INTERFACES

Research Article

www.acsami.org

Comparative Study on Dispersion and Interfacial Properties of Single Walled Carbon Nanotube/Polymer Composites Using Hansen Solubility Parameters

Jing Ma* and Raino Mikael Larsen

Department of Mechanical and Manufacturing Engineering, Aalborg University, 9220 Aalborg, Denmark

ABSTRACT: Dispersion and interfacial strain transfer of single walled carbon nanotubes (SWNTs) are two major challenges for the utilization of SWNTs as reinforcements in polymer composites. Surface modifications could help change the dispersion and interfacial properties. In this study, nanocomposites were fabricated by solution blending 1 wt % SWNTs with various modification (nonmodified, nitric acid functionalized, and amine functionalized SWNTs) and three kinds of polymeric materials (polycarbonate, polyvinylidene fluoride, and epoxy). Chemical compatibilities between SWNTs and solvents or polymers are calculated by the Hansen solubility parameters (HSP) method. The dispersion of the SWNTs in solvents is evaluated by dynamic light scattering. The dispersion of SWNTs in polymers evaluated by a light optical microscope (LOM) generally agrees with the HSP prediction. The strain transfer from the matrix to SWNTs is mainly related to the dispersion, the bundle size, the residual thermal stresses on the sample, and, to lesser degree, the HSP.

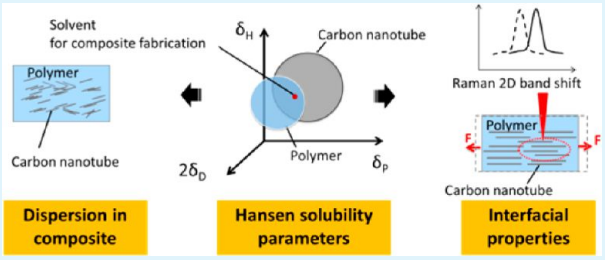

KEYWORDS: *polymer-matrix composites, stress transfer, Hansen solubility parameters, single walled carbon nanotubes, dispersion, dynamic light scattering*

1. INTRODUCTION

The single walled carbon nanotube (SWNT) is a promising material for polymer composite reinforcement; it has impressive mechanical properties with a Young's modulus of 0.32−1.47 TPa, strengths of 10−52 GPa, and toughness of around 770 J/g.[1,2] However, the uniform dispersion of SWNTs in polymer matrix is a critical issue, which limits the applications of nanotube composites.[3] Another major issue for the application of composite is the surface adhesion between the SWNTs and polymers which affects the strain transfer efficiency.[4,5] A great number of studies have been done on modifying the surface of SWNTs, in order to improve the dispersion of SWNTs and the strain transfer efficiency from matrix to SWNTs.[6−8]

Good dispersion and high strain transfer efficiency both require good surface affinity between filler and matrix. The Hansen solubility parameters (HSP) method is widely used to calculate the surface affinity. For some time, HSP have been used to predict the compatibility of polymers and optimize the dispersion of fillers in a polymeric matrix.[9] Launay et al.[10] used HSP to study the affinity between the epoxy resin and different carbon materials including carbon nanotubes. However, a thorough study to correlate the HSP and the dispersion and strain transfer of modified and nonmodified CNT/polymer composite has not yet been reported.

In this study, the effect of surface modification of carbon nanotubes on the properties of composite in different polymer matrix system was investigated. The HSP parameters were determined experimentally for all the involved materials and compatibility between the materials were estimated and compared with the dispersion and strain transfer. The interfacial strain transfer is associated with the dispersion of nanotubes due to the slippage of the nanotube bundles and also the adhesion between nanotubes and polymers. The dispersion of nanotubes in solvents and polymers were studied by dynamic light scattering (DLS) and light optical microscopy (LOM), respectively. In the Raman spectrum of carbon nanotubes, the G band is the most significant peak that comes from the vibration of sp^2 carbon atoms, and the D band appears at about 1350 cm^{-1} and arises from the disordered carbon atoms, providing useful information on the defects. The Raman 2D band (located around 2635 cm^{-1}) is the overtone of the D band, and the position of the 2D band is very sensitive to strain. So the Raman 2D band shift was used to characterize the interfacial strain transfer between SWNTs and the polymeric matrix. At a low strain, in the elastic regime, the Raman 2D peak of SWNTs is very sensitive to mechanical deformation.[11] There is an empirical linear relationship between the Raman 2D band shift ΔNw of SWNT and the applied elastic strain ε, defined as[12−14]

$$\Delta Nw = m\varepsilon \quad (1)$$

Received: October 21, 2012
Accepted: January 30, 2013
Published: January 30, 2013

   dx.doi.org/10.1021/am302407z | ACS Appl. Mater. Interfaces 2013, 5, 1287−1293

Where m is the slope for the line. But at a higher strain, due to weakening of the interfacial adhesion, the Raman response becomes insensitive to strain.

2. HANSEN SOLUBILITY PARAMETERS

In a three-dimensional representation shown in Figure 1, Hansen solubility parameters of a solute (δ_D, δ_P, and δ_H

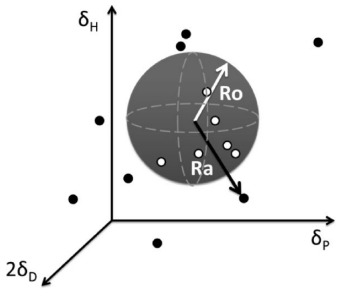

Figure 1. Hansen solubility parameter sphere with dots representing the solvents (white dots good solvents; black dots bad solvents).

represent the dispersion, polar, and hydrogen bonding force parameters, respectively) locate in the geometrical center of the HSP sphere. The radius R_o of the sphere is called the interaction radius. The normal experimental procedure for determining the HSP is based on observation of the interaction between a set of solvents with known HSP and the solute; each solvent is characterized as a bad or good solvent. R_o gives the boundary of the good solvents, which normally are contained within the sphere. HSP distance R_a is the distance between the specified solvent and the center of the solute sphere.

In the Hansen solubility parameters method, a simple composite affinity parameter, relative energy difference (RED) is defined as

$$\mathrm{RED} = R_a/R_o \quad (2)$$

RED values of good solvents are less than 1 indicating strong interactions in most cases; RED values of bad solvents are higher than 1.

However, it is worth noting that deviations can occur at the boundary region. Furthermore, the molecular size may influence the prediction from the HSP model and should be considered in some way. In the HSP method, molecular size influences the interaction radius of the materials; smaller molecules will tend to dissolve more easily than larger ones from a thermodynamic point of view. One way to improve the prediction of the chemical compatibility between a polymers and a solvent is to consider the polymer as a point in the HSP space[15] (i.e. sphere with very small radius of interaction) and the solvent as a sphere with a large interaction radius. Because the polymer is large, it will have a small interaction radius whereas the solvent because it is small it will have a large interaction radius. Due to large amount of work, this inverted system has not been fully explored yet. There are some advantages using this idea in prediction of polymer−polymer miscibility. Polymer miscibility requires that the respective HSP values for the polymers must be very close to each other, thus the R_a distance is considered to be the best measure of the compatibility.[16]

The question now is how the interaction between the various polymers and SWNT should be evaluated. In the present HSP approach, an SWNT is regarded as a polymer. We will use the HSP distance R_a and the degree of overlapping of HSP spheres to compare the interaction between a polymer matrix and various SWNTs. However, no fixed rules have been established to estimate how much overlap is required for good miscibility.

3. MATERIALS AND METHODS

3.1. Materials. The grade A single walled carbon nanotubes were purchased from CarboLex, Inc. and were synthesized by arc-discharge method. The purity of the as-received nanotubes was 50−70% and impurities mainly consist of amorphous carbon and catalyst particles. Average diameter of individual tubes was 1.4 nm, bundle size was approximately 20 nm, and the length was 2−5 μm.

Nonmodified SWNTs (S_1). The nanotubes were annealed in air at 275 °C for 1 h, followed by refluxing in 6 M hydrochloric acid for 6 h to remove the amorphous carbon and the metal catalysts particles. The suspension was washed with water and dried at 100 °C for 24 h. Weight loss was around 50%.

Nitric Acid Functionalized-SWNTs (S_2). A 500 mg portion of nonmodified SWNTs (S_1) were refluxed in 50 mL 5 M nitric acid for 1 h. Then, the SWNTs were washed with de-ionized water and dried at 100 °C for 24 h.

Amine Functionalized-SWNTs (S_3). A 230 mg portion of nitric acid functionalized-SWNTs and 2 g of octadecylamine (ODA) was mixed and heated at 125 °C for 4 days, during which ODA melted and reacted with the nanotubes. Hereafter to remove ODA, the mixture was washed several times by ethanol in an ultrasonic bath and filtered; the temperature was kept above 50 °C during the ultrasonication and filtration. Finally, the SWNTs were dried at 100 °C for 24 h.

The structures of the SWNTs are shown in Figure 2. Evidence of the functionalization was done by attenuated total reflectance (ATR) Fourier transform infrared (FTIR) and is reported in a previous article.[17]

3.2. Solution Preparation of Composites. *PC Composites.* Cyclohexanone (CH-ONE) was ultrasonically mixed with 1 wt % SWNTs with a Dr. Heischel UP400s ultrasonic processor set at 80 W for 2 h. Hereafter, 17−18 g of polycarbonate (PC) purchased from Bayer (trade name: Makrolon Grade M2405F) was added and stirred at 80−90 °C until the PC was dissolved. Furthermore, the compound was heated under vacuum at 130 °C for 3 days to remove CH-ONE.

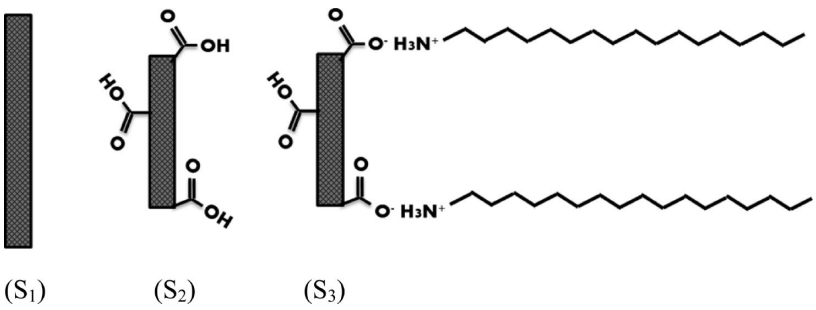

Figure 2. Structure of SWNTs studied in this work.

Injection molding (by a custom made injection molding machine) was carried out at 223 °C, and the mold was heated to 75 °C.

PVDF Composites. For 30 min, 1 wt % SWNTs were ultrasonically dispersed in *N*,*N*-dimethylformamide (DMF) using an 80 W ultrasonic rod generator Heischel UP400s to form a stable suspension. At the same time, PVDF (Sigma-Aldrich 427144-100G) supplied by Aldrich Chemistry, Inc. was dissolved in DMF at 60 °C with constant stirring for 2 h. The carbon nanotubes/DMF suspension was added to the PVDF solution and shear mixed for 30 min at the speed of 5000−6000 rpm. Afterwards, the compound was poured into a large tray to form a very thin layer and dried at 60 °C to remove DMF. TGA measurements showed no traces of DMF. Subsequently, dog bone test specimens (ISO 527-2) were obtained by injection molding (Thermo HAAKE Minijet II) at 260 °C as the melt temperature; the mold was heated to 90 °C, holding at 95 MPa for 10 s.

Epoxy Composites. For 60 min, 1 wt % S_1 and S_2 were dispersed in 99.9% ethanol and S_3 was dispersed in tetrahydrofuran (THF) using an 80 W ultrasonic rod generator Heischel UP400s. The epoxy was mixed using 100 parts LM E20 and 35 parts hardener LM H20 (internal company names). LM E20 is a mixture of bisphenol-A-diglycidylether (BADGE or DGEBA) and minor amounts of bisphenol-F-epichlorhydrin and 2.3-epoxy-propylneodecanoic. LM H20 contains 3-aminomethyl-3,5,5-trimethylcyclohexylamine (IPDA), polyoxyalkylenamin, 2-methyl-1,5-pentandiamine, and benzylalcohol. LM E20 was added and the SWNT/solvent mixture was heated at 60 °C until the solvent was evaporated, and then, the LM H20 hardener was added. Eventually, the sample was cast molded in a silicon mold and cured at 80 °C for 4 h.

3.3. Experimental Methods. *3.3.1. Hansen Solubility Parameters Experiments.* HSP of various SWNTs were determined based on a set of solubility experiments. A very small amount of SWNTs was added into 17 different solvents with known HSP and ultrasonicated for 24 h in a sonication bath; hereafter, the classification into good or bad solvent was made on observation of the sedimentation and the swollen state of SWNTs in the suspension after sonication. A nonlinear optimization toolbox of Matlab based on the goal attainment optimization algorithm was developed to determine the HSP values of polymer and SWNTs.[18] The algorithm simply finds the position and the size of the HSP sphere that will enclose the good solvents and exclude the bad solvents.

3.3.2. Dynamic Light Scattering. The dispersion of SWNTs after 5 min of rod sonication in various solvents was characterized by dynamic light scattering (DLS) performed on a Malvern Zetasizer Nano ZS with a glass cell, using a detection angle of 173°. The test temperature was 20 or 25 °C, and the viscosities of the solvents at the measuring temperature were provided to the software.

The carbon nanotubes have very high aspect ratio and could exist as isolated nanotubes, nanotube bundles, and agglomerated carbon nanotubes. The Zetasizer measures the hydrodynamic particle size. The hydrodynamic diameter is the size of a sphere that has the same diffusion behavior as the measured particle; it is an effective diameter of the nanoparticles in a liquid environment. This technique only estimates the degree of dispersion; it is impossible to get the information on the shape and real size of carbon nanotubes. However, several authors have used the technique on CNT dispersions as an indication of the bundle size of the CNTs.[19−23] As shown in Figure 3, the hydrodynamic size depends not only on the diameter of the particle core but also on the surface structure and the concentration and type of ions in the medium as well. Polydispersity index (PDI) is calculated as an indicator of the homogeneity of the sample, it corresponds to the square of the normalized standard deviation of an underlying Gaussian size distribution. PDI ranges from 0 to 1, and small PDI values indicate a narrow size distribution.

3.3.3. Light Optical Microscopy. The dispersion of carbon nanotubes in polymer matrix was characterized by LOM on thin composite sections with a thickness of about 15 μm, which were cut from the bulk dog bone specimens. The photographs were taken under the same condition, i.e., the same light intensity and exposure.

3.3.4. Interfacial Strain Transfer. The composites were tested in a Renishaw Invia Raman Microscope with a He−Ne laser (632.8 nm) through a 5× objective lens, forming a laser spot on the sample of about 20−40 μm in diameter.

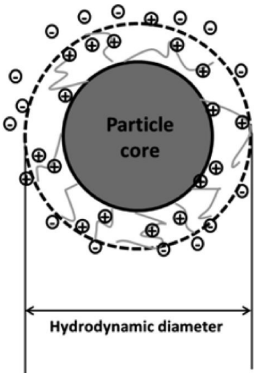

Figure 3. Hydrodynamic particle size.

Strain induced changes in the Raman peak around 2635 cm^{-1} (so called 2D band) have been observed for individual single walled carbon nanotubes and SWNT/polymer composites.[24,25] Because the applied strain introduced changes on the C−C bond vibrations and hence strongly affects the Raman spectrum, there is a linear downshift of the 2D band with tensile strain, and the slope of the shift with strain is used to evaluate the strain transfer efficiency in the composite.[11,13,25,26]

The small dog bone specimens were loaded in a custom-made tensile test rig placed on the microscope table. The laser polarization was parallel to the loading direction; there was an analyzer also with the polarization direction parallel to the loading direction. The specimen was gradually loaded up to different strains, and Raman spectra were taken at each strain level.

3.3.5. Creep Testing. The creep behavior of the three neat polymers were experimentally tested at room temperature on an Instron 5944 tensile testing machine equipped with an extensometer; the creep strain was measured at a constant tensile load of 40 MPa and holding for 20 min.

4. RESULTS AND DISCUSSION

4.1. Dispersion of SWNTs in Solvents. It was observed that S_1 and S_2 were easily dispersed in CH-ONE and DMF and formed a stable suspension, but S_3 was very difficult to disperse in these two solvents. However, S_3 was very easily dispersed in THF and the dispersion was very stable. Whereas S_1 and S_2 in EtOH were more difficult to disperse, the dispersions were only stable for some days and carbon nanotubes (CNTs) settled slowly to the bottom of the container.

The DLS results of the SWNTs dispersed in the solvents used for the composite processing are presented in Table 1; we note that, through surface modification, the oxidized nanotube S_2 has a smaller hydrodynamic particle size and PDI than S_1 in each group, while S_3 showed the largest hydrodynamic particle size in each group because of the long hydrocarbon chains grafted onto the surface of the nanotube.

Table 1. DLS Results of SWNTs in the Solvents Used for Composite Fabrication

	S_1		S_2		S_3	
	Z-ave (nm)	PDI	*Z*-ave (nm)	PDI	*Z*-ave (nm)	PDI
CH-ONE	471.3	0.507	356.6	0.391	1390	0.464
DMF	192.7	0.368	175.8	0.345	464.6	0.779
EtOH	322.2	0.728	260.5	0.496		
THF					336.9	0.338

Table 2. Solubility of SWNTs in Various Solvents

solvents	δ_D[a]	δ_P[a]	δ_H[a]	S_1 S[b]	S_1 RED	S_2 S[b]	S_2 RED	S_3 S[b]	S_3 RED
methanol	15.1	12.3	22.3	1	1.00	1	0.97	0	5.99
ethanol	15.8	8.8	19.4	1	0.70	1	0.93	0	4.53
2-propanol	15.8	6.1	16.4	0	0.65	1	1.00	0	3.34
acetone	15.5	10.4	7.0	0	1.00	1	0.77	0	2.20
tetrahydrofuran	16.8	5.6	8.0	1	0.84	0	1.00	1	0.46
cyclohexanone	17.8	6.3	5.1	1	0.98	1	1.04	0	1.04
ethyl acetate	15.8	5.3	7.2	1	1.00	0	1.08	1	0.83
acetonitrile	15.3	18.0	6.1	0	1.35	1	0.60	0	4.72
dimethylformamide	17.4	13.7	11.3	1	0.64	1	0.33	0	3.42
diethylethenamine	17.8	0.4	1.0	0	1.53	0	1.59	0	2.43
dicloromethan	18.2	6.3	6.1	0	0.88	0	1.00	0	1.06
chloroform	17.8	3.1	5.7	1	1.05	0	1.23	1	0.92
tetrachloromethane	17.8	0.0	0.6	0	1.58	0	1.63	0	2.81
hexane	14.9	0.0	0.0	0	1.77	0	1.71	0	3.25
decahydronaphthalene	18.8	0.0	0.0	0	1.61	0	1.66	0	3.18
benzene	18.4	0.0	2.0	0	1.46	0	1.58	0	2.57
xylol	17.8	1.0	3.1	0	1.34	0	1.47	0	1.95

[a]The HSP are in units of $MPa^{1/2}$. Refs 15 and 27. [b]S represents the solubility. "1" and "0" stand for the good and bad solvent, respectively.

The PDI of S_3 in CH-ONE and THF is small (0.464 and 0.338) which means that the distribution of the particles is quite narrow. While S_3 in DMF shows a large PDI of 0.779 and thus the particle size distribution is boarder, some large agglomerates are very likely to appear.

The solubility of SWNTs in solvents with known HSP is presented in Table 2, and the relative energy difference (RED) values of SWNTs in solvents are also listed.

In the HSP experiments, the solubility of SWNTs is determined by visual observation of the suspension. The solvents for stable dispersion of nanotubes are called good solvents. Otherwise, the solvents that lead to CNT sedimentation are bad solvents. As can be seen from Table 2, CH-ONE is a bad solvent for S_3, a good solvent for S_1 and S_2, and the results are in good agreement with the DLS results. DMF is a good solvent for S_1 and S_2, but a bad solvent for S_3 with RED of 3.42; RED of S_2 (0.33) is the smallest indicating the best compatibility. S_1 and S_2 dispersed well in ethanol, S_3 also dispersed well in THF, and RED for S_3 in THF (0.46) indicates the best compatibility in this group. The HSP method helps to quantify the theory "like dissolves likes" and the interaction between two materials. It was found that the interaction between CNT and solvent quantified by the HSP method agrees well with the dispersion of the CNT in solvents tested by the DLS method.

4.2. Dispersion of SWNTs in Composites. The solubility of epoxy resin was also studied by HSP experiments as listed in Table 3. Table 4 illustrates the HSP results of CNT and polymers. In this work both the overlapping region of the spheres and the HSP distance R_a (shown in Figure 4) are considered when trying to estimate the interaction between the polymer and the CNT fillers. The R_a between S_3 and PC is small (7.75), the overlap region between S_3 and PC is large, the HSP sphere of S_3 is completely included in the HSP sphere of PC, so the compatibility between S_3 and PC might be the best in this group. The compatibilities of S_1 and S_2 with PVDF are good, and S_2 (shortest R_a of 3.45) shows the best compatibility, while S_3 (longest R_a of 8.64) shows the worse compatibility. The HSP sphere of PVDF is included in S_1 and S_2; however, there is no overlap region between S_3 and PVDF. In epoxy (Table 3), S_3 may have very good compatibility with a very small R_a of 5.24, while S_1 and S_2 show the larger R_a of 12.71 and

Table 3. Solubility of Epoxy Resin in Various Solvents

solvents	δ_D[a]	δ_P[a]	δ_H[a]	epoxy resin S[b]
methanol	15.1	12.3	22.3	0
ethanol	15.8	8.8	19.4	0
2-propanol	15.8	6.1	16.4	0
acetone	15.5	10.4	7.0	1
tetrahydrofuran	16.8	5.6	8.0	1
cyclohexanone	17.8	6.3	5.1	1
ethyl acetate	15.8	5.3	7.2	1
acetonitrile	15.3	18	6.1	1
dimethylformamide	17.4	13.7	11.3	1
diethylethenamine	17.8	0.4	1.0	0
dicloromethan	18.2	6.3	6.1	1
chloroform	17.8	3.1	5.7	1
tetrachloromethane	17.8	0.0	0.6	1
hexane	14.9	0.0	0.0	0
decahydronaphthalene	18.8	0.0	0.0	0
benzene	18.4	0.0	2.0	1
xylol	17.8	1.0	3.1	1

[a]The HSP are in units of $MPa^{1/2}$. Refs 15 and 27. [b]S represents the solubility. "1" and "0" stand for the good and bad solvent, respectively

Table 4. Estimates for HSP, Interaction Radius R_o of S_1, S_2, S_3, and Polymers

material	δ_D[a]	δ_P[a]	δ_H[a]	R_o[a]
S_1	19.4	10.4	15.2	11.3
S_2	16.1	12.8	13.4	9.1
S_3	17.0	4.7	7.1	2.9
PC[b]	19.1	10.9	5.1	12.1
PVDF[c]	17.1	12.6	10.6	5.0
epoxy resin[d]	16.5	8.8	4.0	9.8

[a]The HSP and R_o are in units of $MPa^{1/2}$. [b]Using published data in ref 15. [c]Calculated using published data in ref 28. [d]Using experimental data in Table 3.

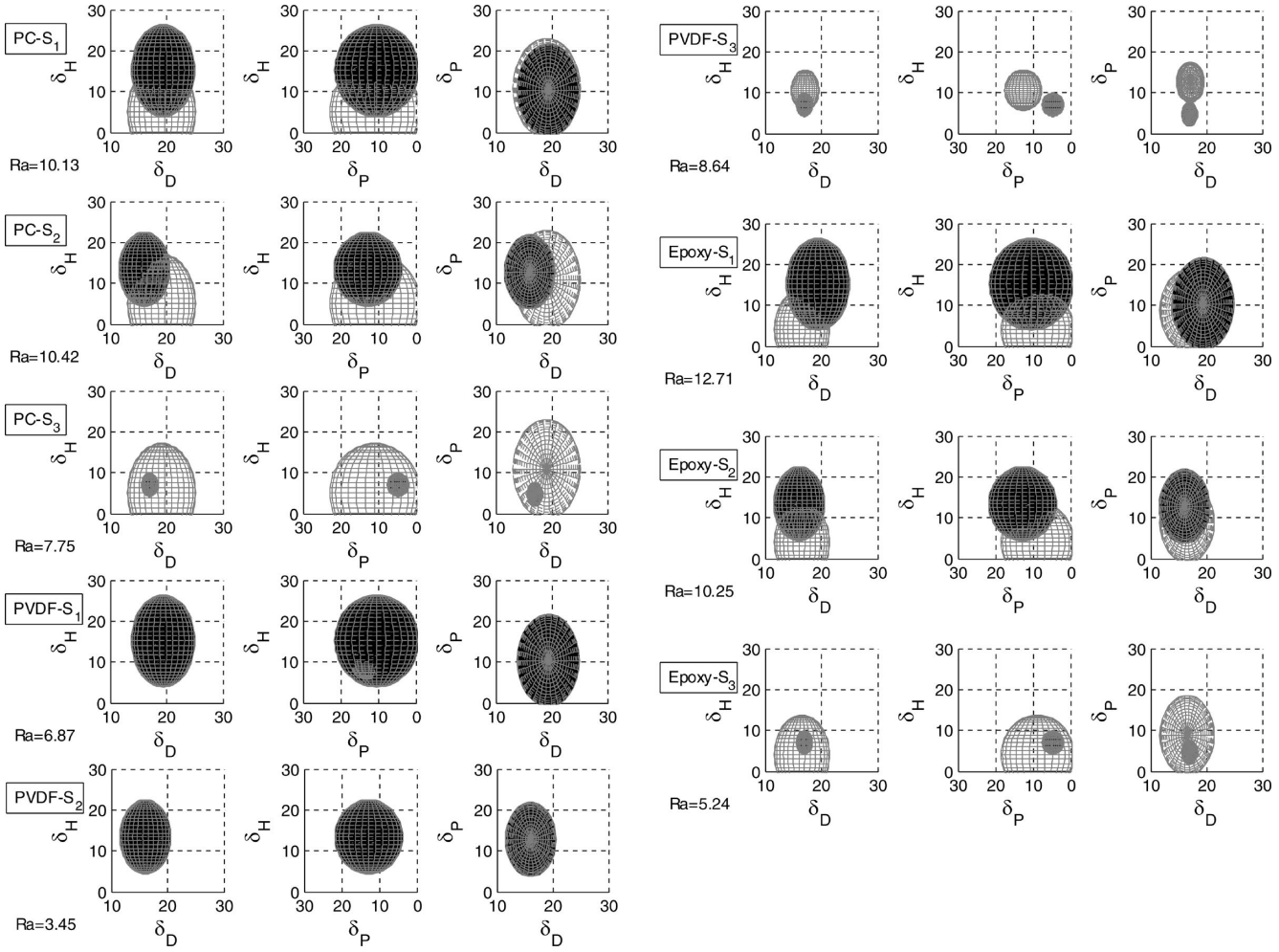

Figure 4. Calculated HSP graphs (transparent sphere polymer; black sphere carbon nanotube). The R_a values are shown to the left of the HSP graphs.

10.25. Taking a look at the overlapping region, the interaction sphere of S_3 is all included in epoxy, which indicates good compatibility.

The dispersion of SWNTs in composites was evaluated by LOM as shown in Figure 5. Due to the high contrast between the nanotube aggregates and the transparent polymer, LOM was very suitable for observation of nanotube agglomerates. The nanotube S_3 dispersed very homogenously in PC; S_1 and S_2 form a few agglomerates in PC. In PVDF composites, S_1 and S_2 are dispersed evenly, and there are no obvious aggregates in them. S_3 dispersed badly with aggregate size of about 50 μm. In the epoxy composites, S_1 formed several aggregates around 20–30 μm; however, after nitric acid treatment, S_2 dispersed even more poorly in epoxy and a large amount of aggregates at the size of over 100 μm were formed. S_3 dispersed uniformly in epoxy and without large aggregates. In the latter case, THF was used as the solvent.

The dispersion of SWNTs in polymer agree with the predictions by HSP method. For instance, in S_3–PC and S_3–epoxy, the dispersion of SWNTs is very homogenous and has good compatibility, S_3–PVDF, S_1–epoxy, and S_2–epoxy samples show poor dispersion and bad compatibility. Ultrasonication causes the carbon nanotubes to de bundle in the solvents,[29] but after mixing with the polymer solution and during the evaporation of the solvent, the nanotubes tend to re-agglomerate.[30−32] Strong surface affinity between nanotubes and polymer hinder the re-agglomeration of nanotubes. This indicates that in our study the compatibility with the polymer is more important than compatibility with the solvent used during the manufacturing.

4.3. Stress Transfer. In our study, Raman is used to characterize the interfacial strength, i.e. adhesion. The slope of the Raman 2D peak shift and the maximum down shift under applied tensile strain can be used as a measure of the average strain transfer from polymer to SWNTs. With a stronger interface, the slope of the Raman 2D peak shift will be higher and larger down shift will occur under the applied strain. There are many factors that may account for the strain transfer, but in general, the interfacial adhesion between SWNT and matrix plays an important role; a large contact area is another key factor. Figure 6 illustrates the Raman 2D band shift of SWNTs when the composites are exposed to tensile loads.

For each polymer group, the strain transfer efficiency of S_2 and S_3 in polymer is improved compared with the nonmodified SWNT filled composite, where S_2 shows the best strain transfer. Nitric acid treatment causes the debundling of SWNTs as also indicated by DLS measurements. The area of the interphase increases when the SWNT debundling occurs; hence, the strain transfer efficiency increases. Meanwhile, with the functional −COOH groups on the surface of SWNTs, stronger adhesion might be created at the interface. A model predicted that loads are transferred onto nanotubes through the pinning at sites of

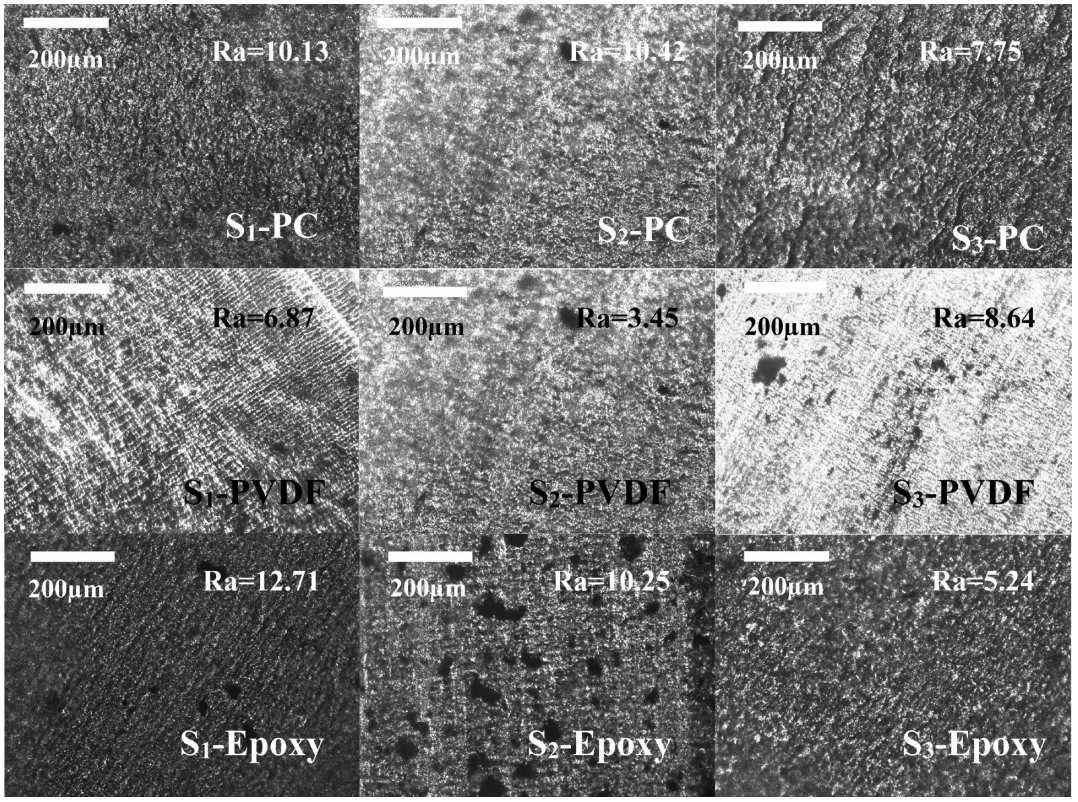

Figure 5. Comparison of light optical microscope images of the different composites and the HSP R_a distance between nanotube and polymer.

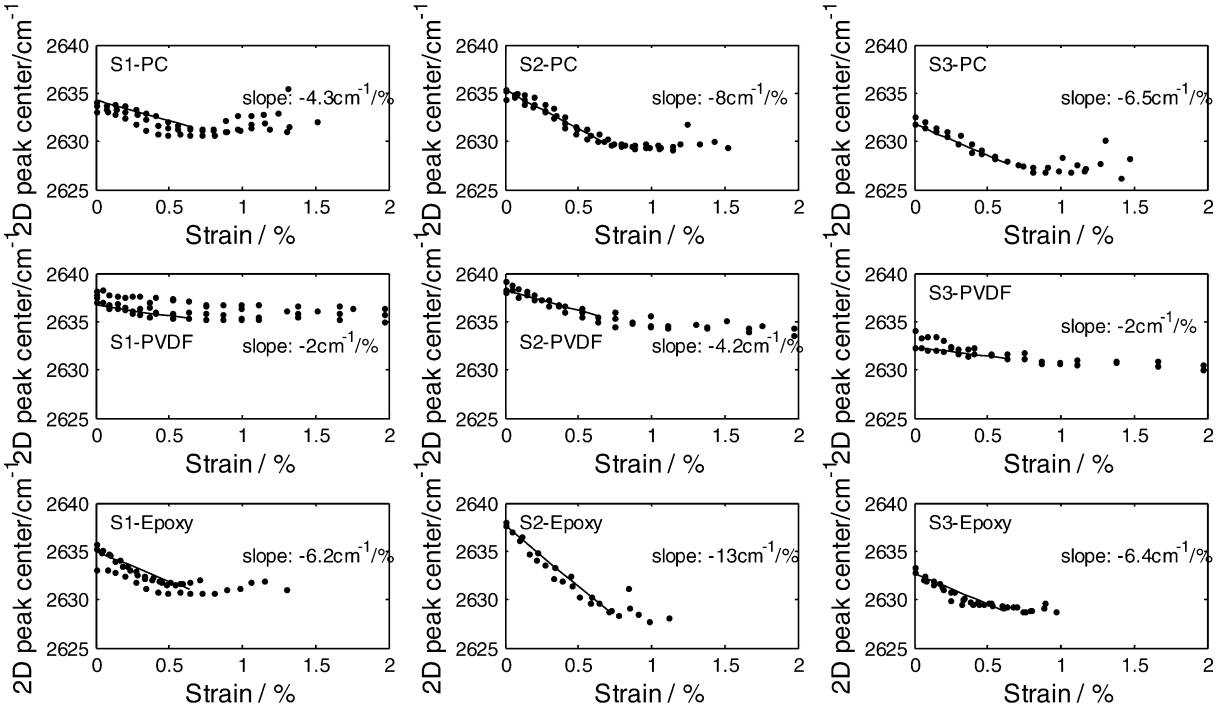

Figure 6. Comparison of Raman 2D band shifts of SWNT composites under tension.

defects, surface adsorbents, or other irregularities at the interface that can enhance the local adhesion to the matrix.[33] The improved strain transfer for the ODA-functionalized SWNT in PC and epoxy compared with S_1 may be due to the functional groups and stronger surface affinity as indicated by the HSP experiments.

Generally, the strain transfer of SWNTs in epoxy is the best, while that in PVDF is the worst. Covalent bonds are easily formed between the functional groups of SWNTs and thermoset polymer epoxy, and the SWNTs become part of the network of the cross-linked chains; therefore, the strain transfer is enhanced.[34,35] The best transfer is observed for the

S_2−epoxy sample despite the existence of agglomerates. For thermoplastics PC (an amorphous polymer) and PVDF (a semicrystalline polymer), the noncovalent interactions (such as van der Waals forces and dipole interactions) at the PC-SWNT and PVDF-SWNT interfaces is relatively weak; the adhesion at the interface is mainly due to frictional forces caused by residual thermal stresses after injection molding. These residual stresses will decrease as a result of stress relaxation of the matrix and thus decrease the strain transfer efficiency.[36] From the creep test of the three neat polymers at room temperature, it was found that at a constant tensile load of 40 MPa and holding for 20 min, the creep strains of PC, PVDF, and epoxy were 0.5%, 4.2%, and 0.6%, respectively. Thus, the better strain transfer of PC compared to PVDF is mainly due to better viscoelastic properties of the PC. Our observations indicate that the strain transfer is only weakly linked to the chemical compatibility as indicated by the HSP method but is mainly affected by the SWNT bundle size, bonding nature and frictional forces caused by the residual thermal stresses.

5. CONCLUSIONS

This paper compares the chemical compatibility, dispersion, and strain transfer of three different modified single walled carbon nanotubes in three different polymer (PC, PVDF, Epoxy) composites.

The dispersion of carbon nanotubes in solvents used for composite fabrication was characterized by dynamic light scattering. Nitric acid-functionalized nanotubes in solvents show smaller particle size than nonmodified nanotubes, while the particle size of amine-functionalized nanotubes in solvents is larger due to the attached hydrocarbon chains. RED values of SWNTs in different solvents calculated by Hansen solubility parameters method generally agreed with the dynamic light scattering results.

The dispersions of the SWNTs in polymers are in good agreement with the HSP compatibility predictions between SWNTs and polymer. The strong surface affinity between nanotubes and polymer hindered the re-agglomeration of nanotubes during the solvent evaporation, and in cases with poor compatibility, re-agglomeration takes place. Strain transfer efficiency of SWNTs is improved through surface modification. The strain transfer is not reflected by the HSP compatibility but highly related to the debundling of carbon nanotubes, the surface affinity, and the bonding nature. Strain transfer is also related to thermal residual stresses causing frictional stresses at the interface. These residual stresses decrease during aging depending on the viscoelastic properties of the polymer.

AUTHOR INFORMATION

Corresponding Author

*E-mail: jingma1984@yahoo.com.cn. Tel.: +45 9940 9296.

Notes

The authors declare no competing financial interest.

REFERENCES

(1) Ruoff, R. S.; Lorents, D. C. *Carbon* **1995**, *33*, 925−930.
(2) Yu, M. F.; Files, B. S.; Arepalli, S.; Ruoff, R. S. *Phys. Rev. Lett.* **2000**, *84*, 5552−5555.
(3) Ma, P. C.; Siddiqui, N. A.; Marom, G.; Kim, J. K. *Composites Part A* **2010**, *41*, 1345−1367.
(4) Yang, M. J.; Koutsos, V.; Zaiser, M. *J. Phys. Chem. B* **2005**, *109*, 10009−10014.
(5) Xie, L.; Xu, F.; Qiu, F.; Lu, H. B.; Yang, Y. L. *Macromolecules* **2007**, *40*, 3296−3305.
(6) Hwang, G. L.; Shieh, Y. T.; Hwang, K. C. *Adv. Funct. Mater.* **2004**, *14*, 487−491.
(7) Ramanathan, T.; Liu, H.; Brinson, L. C. *J. Polym. Sci., Part B: Polym. Phys.* **2005**, *43*, 2269−2279.
(8) Zhu, J.; Kim, J. D.; Peng, H.; Margrave, J. L.; Khabashesku, V. N.; Barrera, E. V. *Nano Lett.* **2003**, *3*, 1107−1113.
(9) Lafaurie, A.; Azema, N.; Ferry, L.; Lopez-Cuesta, J. M. *Powder Technol.* **2009**, *192*, 92−98.
(10) Launay, H.; Hansen, C. M.; Almdal, K. *Carbon* **2007**, *45*, 2859−2865.
(11) Cooper, C.; Young, R.; Halsall, M. *Composites Part A* **2001**, *32*, 401−411.
(12) Wood, J. R.; Wagner, H. D. *Appl. Phys. Lett.* **2000**, *76*, 2883−2885.
(13) Zhao, Q.; Wagner, H. D. *Philos. Trans. R. Soc. A* **2004**, *362*, 2407−2424.
(14) Wood, J. R.; Zhao, Q.; Frogley, M. D.; Meurs, E. R.; Prins, A. D.; Peijs, T.; Dunstan, D. J.; Wagner, H. D. *Phys. Rev. B* **2000**, *62*, 7571−7575.
(15) Hansen, C. M. *Hansen solubility parameters: a user's handbook*, 2nd ed.; CRC Press: Boca Raton, 2007; Appendix .
(16) Hansen, C. M. *Prog. Org. Coat.* **2004**, *51*, 109−112.
(17) Larsen, R. *J. Mater. Sci.* **2009**, *44*, 799−807.
(18) Ma, J.; Zhou, L. L. *Polym. Bull.* **2012**, *68*, 1053−1063.
(19) Murdock, R. C.; Braydich-Stolle, L.; Schrand, A. M.; Schlager, J. J.; Hussain, S. M. *Toxicol. Sci.* **2008**, *101*, 239−253.
(20) Kuan, H. C.; Ma, C. C. M.; Chang, W. P.; Yuen, S. M.; Wu, H. H.; Lee, T. M. *Compos. Sci. Technol.* **2005**, *65*, 1703−1710.
(21) Datsyuk, V.; Landois, P.; Fitremann, J.; Peigney, A.; Galibert, A. M.; Soula, B.; Flahaut, E. *J. Mater. Chem.* **2009**, *19*, 2729−2736.
(22) Lucas, A.; Zakri, C.; Maugey, M.; Pasquali, M.; Schoot, P.; Poulin, P. *J. Phys. Chem. C* **2009**, *113*, 20599−20605.
(23) Badaire, S.; Poulin, P.; Maugey, M.; Zakri, C. *Langmuir* **2004**, *20*, 10367−10370.
(24) Cronin, S. B.; Swan, A. K.; Unlu, M. S.; Goldberg, B. B.; Dresselhaus, M. S.; Tinkham, M. *Phys. Rev. Lett.* **2004**, 93.
(25) Schadler, L. S.; Giannaris, S. C.; Ajayan, P. M. *Appl. Phys. Lett.* **1998**, *73*, 3842−3844.
(26) Gao, Y.; Li, L. Y.; Tan, P. H.; Liu, L. Q.; Zhang, Z. *Chin. Sci. Bull.* **2010**, *55*, 3978−3988.
(27) Barton, A. F. M. *CRC handbook of solubility parameters and other cohesion parameters*, 2nd ed.; CRC Press: Boca Raton, 1991; p 104.
(28) Bottino, A.; Capannelli, G.; Munari, S.; Turturro, A. *J. Polym. Sci., Part B: Polym. Phys.* **1988**, *26*, 785−794.
(29) Niyogi, S.; Hamon, M. A.; Perea, D. E.; Kang, C. B.; Zhao, B.; Pal, S. K.; Wyant, A. E.; Itkis, M. E.; Haddon, R. C. *J. Phys. Chem. B* **2003**, *107*, 8799−8804.
(30) Xu, J. B.; Zhao, T. S. *J. Power Sources* **2010**, *195*, 1071−1075.
(31) Tang, X. G.; Hou, M.; Ge, L.; Zou, J.; Truss, R.; Yang, W.; Yang, M. B.; Zhu, Z. H.; Bao, R. Y. *J. Appl. Polym. Sci.* **2012**, *125*, E592−E600.
(32) Li, Y.; Fernandez-Recio, L.; Gerstel, P.; Srot, V.; van Aken, P. A.; Kaiser, G.; Burghard, M.; Bill, J. *Chem. Mater.* **2008**, *20*, 5593−5599.
(33) Leeuw, T. K.; Tsyboulski, D. A.; Nikolaev, P. N.; Bachilo, S. M.; Arepalli, S.; Weisman, R. B. *Nano Lett.* **2008**, *8*, 826−831.
(34) Moniruzzaman, M.; Du, F. M.; Romero, N.; Winey, K. I. *Polymer* **2006**, *47*, 293−298.
(35) Zhu, J.; Kim, J. D.; Peng, H. Q.; Margrave, J. L.; Khabashesku, V. N.; Barrera, E. V. *Nano Lett.* **2003**, *3*, 1107−1113.
(36) Thomsen, J. S.; Pyrz, R. *Compos. Sci. Technol.* **1999**, *59*, 1375−1385.